Graphene-based all-optical modulators

Chuyu ZHONG[1,2], Junying LI[3], Hongtao LIN (✉)[1,2]

1 Key Laboratory of Micro-Nano Electronics and Smart System of Zhejiang Province, College of Information Science
and Electronic Engineering, Zhejiang University, Hangzhou 310027, China
2 School of Microelectronics, Zhejiang University, Hangzhou 310027, China
3 College of Optical-Electrical and Computer Engineering, University of Shanghai for Science and Technology, Shanghai 200093, China

Abstract All-optical devices, which are utilized to process optical signals without electro-optical conversion, play an essential role in the next generation ultrafast, ultralow power-consumption optical information processing systems. To satisfy the performance requirement, nonlinear optical materials that are associated with fast response, high nonlinearity, broad wavelength operation, low optical loss, low fabrication cost, and integration compatibility with optical components are required. Graphene is a promising candidate, particularly considering its electrically or optically tunable optical properties, ultrafast large nonlinearity, and high integration compatibility with various nanostructures. Thus far, three all-optical modulation systems utilize graphene, namely free-space modulators, fiber-based modulators, and on-chip modulators. This paper aims to provide a broad view of state-of-the-art researches on the graphene-based all-optical modulation systems. The performances of different devices are reviewed and compared to present a comprehensive analysis and perspective of graphene-based all-optical modulation devices.

Keywords graphene, saturable absorption, low power consumption, all-optical modulation

1 Introduction

The continuously growing internet data traffic has led to a burgeoning demand for faster and more energy-efficient information processing technology, which has prompted extensive research on ultrafast, ultralow power consuming, and miniature modulators [1,2]. The state-of-the-art electro-optical modulator (EOM) has recorded significant

progress recently. The thin-film $LiNbO_3$-based EOM has a modulation bandwidth close to or exceeding 100 GHz with a modulation speed of over 100 Gb/s and energy dissipation of tens or hundreds of femto-joules per bit [3,4]. Silicon-based modulators also have modulation speeds higher than 100 Gb/s with a 3-dB bandwidth of over 50 GHz [5]. Moreover, silicon-organic-hybrid modulators can function at a 3-dB bandwidth higher than 100 GHz [6]. Through strong nanoscale local-field enhancement, plasmonic phase modulators [7–9] could be scaled down to the micron level while maintaining femto-joule energy consumption and modulation speeds of hundreds-of-Gb/s. Although significant progress has been achieved recently, the intrinsic limitation from the parasitic capacitance and resistance in the electric circuit, as well as the energy consumption from the electro-optical conversion still limit their ultimate performance. It is difficult to simultaneously elevate the modulation rate up to Tb/s and impress the power dissipation down to femto-joules per bit.

All-optical modulators (AOMs), where the modulation is realized by using a pump light to control the probe light [10–13], have a great potential to overcome the bottleneck of the EOM. Compared to the EOM, AOMs could eliminate the electro-optical-electro conversion and achieve lower power consumption with a larger bandwidth [14]. A variety of photonic platforms have been applied to achieve all-optical modulation via ultrafast nonlinear interaction [15–18]. Materials with ultra-high nonlinearity play a key role in determining the ultimate speed and energy consumption limit of AOMs, and resonance or plasmonic structures could be assisted to achieve a high ON/OFF ratio and small device footprint. In 2004, by harnessing the optical plasma dispersion effect induced by resonance-enhanced two-photon absorption, silicon ring resonator AOMs were first reported by Michal Lipson's group with a response time of 200 ps and an energy consumption of 25 pJ/bit [15]. Later in 2010, Nozaki et al. fabricated an InGaAsP photonic crystal cavity with a

record performance of 0.42 fJ/bit and a 20 ps switching time [19]. Leveraging the four-wave mixing (FWM) phenomenon in the As_2S_3 [20] or silicon [21] waveguide, all-optical logic gate devices with a speed of 160 Gb/s and a power consumption of 65 fJ/bit have been developed. Recently, metal-polymer hybrid epsilon-near-zero materials have also been integrated into silicon slot ring resonators or plasmon nanocavities for all-optical switching and logical devices [22–25]. All-optical programmable logic arrays based on semiconductor optical amplifiers could operate at a speed of 40 Gb/s [26]. Ultralow power-consumption and ultra-compact devices with response times of tens of picoseconds were obtained. However, the trade-off between the large nonlinearity and ultrafast switching limited the ultimate performance of the existing all-optical modulation technology, and new materials and device platforms for AOMs are yet to be explored [13].

The intriguing properties of two-dimensional (2D) materials [27–31] have attracted significant attention for application in emerging ultrafast photonic devices, including mode-lock lasers [32–40], photodetectors [41–46], and modulators [47–51]. Among those layered materials, graphene [52] is a highly versatile material that offers exceptional optical and electrical properties, particularly strong nonlinearity and ultrafast relaxation. With all these extraordinary properties, graphene has been studied extensively for application in optical devices such as ultrafast lasers [53–57], detectors [58–60], broadband modulators [61–65], switches [66,67], polarizers [68], and solar cells [69]. In 2011, Xiang Zhang's group first reported a graphene-based electro-optic silicon modulator [63], where gating electrodes modulated the absorption of the graphene. A 3-dB bandwidth of 1.2 GHz had been achieved with an energy consumption of 880 fJ/bit. In 2015, ring resonators with two layers of graphene acting as two electrodes of a capacitor realized a 3-dB bandwidth of 30 GHz with a power consumption of 800 fJ/bit [65]. In 2018, graphene–silicon Mach-Zehnder interferometer (MZI) modulators operating in the gigahertz regime with a modulation efficiency of 0.28 V·cm and an operating speed of 10 Gbit/s were demonstrated [70]. The photonic crystal cavity was also introduced in the graphene-based EOM, reported in 2019 by Xinliang Zhang's group with a bandwidth reaching 12 GHz [71]. In the same year, an EOM based on graphene integrated with photonic crystal fiber was reported. A broadband response from 1150 to 1600 nm and a large modulation depth of ~20 dB/cm at 1550 nm under a low gate voltage of ~2 V were realized [72]. Moreover, 2D materials have application prospects in all-optical modulation [73]. Recently, Masaya Notomi's group fabricated an ultrafast graphene-loaded ultra-compact plasmonic slot-waveguide all-optical switching device with a switching energy of 35 fJ and a switching time of 0.26 ps, which corresponded a bandwidth of 1.2 THz [1]. These signs of progress and the potential for complementary metal oxide semiconductor (CMOS)-

compatible integration capability highlight graphene as an auspicious material for application in AOMs.

In this review, we focus on graphene as a great candidate for application in AOMs. In the following sections, we discuss the recent progress in graphene-based AOM research. First, we briefly introduce the status of graphene photonics. In Section 2, we discuss the nonlinear effects of graphene in the all-optical modulation scheme. In Section 3, we present the latest experimental demonstrations of graphene-based AOMs. Finally, we conclude our paper with current challenges and outlook in Section 4.

2 Optical modulation in graphene

Graphene is a single-layered atomic crystal. Its Dirac cone type electronic band structure [74] exhibits linear energy dispersion without a bandgap [75], which accounts for its extraordinary electrical and optical characteristics. The carrier mobility at room temperature can reach 2×10^5 $cm^2/(V \cdot s)$ [76,77], which is essential for ultrafast modulation. The absorption coefficient, $\pi \alpha$, of mono-layered graphene from the visible to the mid-infrared region (300–6000 nm) is 2.293% [78], which supports ultra-broadband operation [79]. The most significant property for application in modulators is its ultralow threshold of saturable absorption and ultrashort relaxation time, which has been experimentally validated to be in the range of femtoseconds ((8 ± 3) fs) to picoseconds (1.63 ps) [80,81]. Furthermore, graphene is compatible with the CMOS fabrication process and could be integrated with various materials and photonic structures, which guarantees tunable light–matter interaction. The four nonlinear effects involved in the graphene-based AOM are discussed in the following subsections and are summarized in Fig. 1.
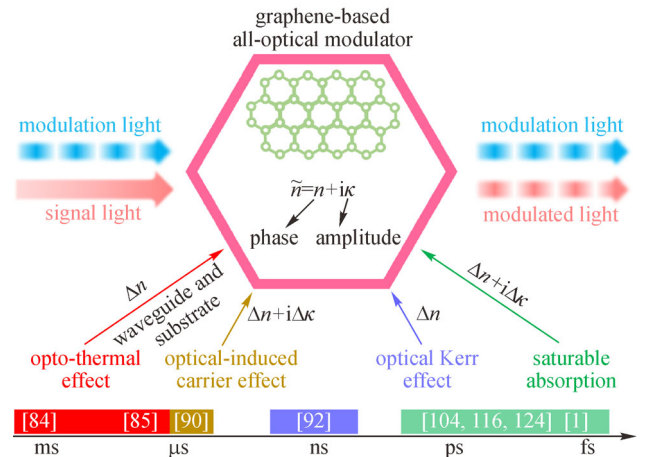

Fig. 1 Mechanisms and corresponding response time of referenced graphene-based AOMs. The modulation of complex refractive index $\tilde{n}$ can be concluded into the modulation of the real part of refractive index (n for phase modulation) and imaginary part of refractive index (k for amplitude modulation)

2.1   Opto-thermal effect

Light modulation or switching by thermal tuning is widely utilized in silicon photonic circuits [82]. Graphene possesses an ultra-high thermal conductivity in the range of 4840–5300 W/mK due to the fast phonon transportation in its lattices [83]. The excited carriers can transfer their energy to phonons during the relaxation process, thereby elevating the temperature of the material. Therefore, when integrated with optical waveguides, graphene can be used as an efficient and compact heat generator and conductor for optical-induced thermo-optic modulation. The heat generated from light absorption in graphene can be transferred to surrounding materials, which changes the refractive index of the material and, consequently, results in the realization of phase modulation. Based on both the microfiber [84,85] and on-chip [86] platform, the photo-thermal effect of graphene was utilized to achieve phase modulation. The phase modification could be achieved with a proper choice of substrate or encapsulant. The time constant for the heat dissipation is typically low, and the switching time ranges from micro to milliseconds, which is limited by phonon coupling between graphene and the surrounding materials. The cooling time of the hBN-graphene-hBN sandwich structure was reported to be less than 10 ps, which contributes to the out-of-plane heat transfer through electron-hyperbolic phonon polariton coupling [87]. This exciting result revealed a potential path to ultrafast opto-thermal modulation.

2.2   Optical-induced carrier effect

The optical illumination of graphene and its surrounding materials can produce electron–hole pairs. The carrier pairs are separated between the interface of graphene and its contacted semiconductors. These optical-induced carriers could accumulate and change the real and imaginary parts of the refractive index for both materials through the plasma dispersion effect [88]. The modulation of the THz wave is achieved by integrating graphene with silicon [89] or germanium [90]. Subsequently, the photon-induced electron–hole pairs generated in the illuminated area of silicon or germanium are transferred to graphene, which changes the conductivity of graphene and silicon/germanium, thereby resulting in the modulation of the THz wave absorption. The lifetime of interlayer carriers is usually in the range of nano- to micro-seconds with a low power threshold. However, the response time is still significantly below the requirement for ultrafast all-optical modulation.

2.3   Optical Kerr effect

To achieve high-speed all-optical modulation, ultrafast nonlinear phenomena, such as the optical Kerr effect, can be induced. The Kerr effect is induced by separating photon-induced electron–hole pairs, and the index change linearly varies with the pump power [13]. This effect could be expressed by the power-induced change of the real part of the refractive index: $\Delta n = n_0 + n_2 \Delta I$ [13], where n_0 is the linear refractive index, n_2 is the nonlinear refractive index, and ΔI is the change in the pump light intensity. Graphene delivers a nonlinear refractive index of $n_2 \approx 10^{-7}$ cm^2/W, which is several orders of magnitude larger than those of bulk dielectrics [91]. By integrating graphene into an MZI based on an optical fiber system, the Kerr-effect-induced refractive index change in graphene was used to modify the phase difference between interference arms and to, therefore, fine-tune the output transmission, which was applied for signal processing with a response time in the order of nanoseconds [92].

2.4   Saturable absorption

Another type of ultrafast all-optical modulation is achieved by nonlinear saturable absorption, which was widely used for graphene-based AOMs. The saturable absorption in graphene is due to the Pauli blocking effect [93]. When a pump light with a photon energy twice the Fermi energy level (or chemical potential) of graphene is injected into a graphene-based AOM, the electrons in graphene are excited from the valence band to the conduction band [94,95]. The excitation process of the carriers leads to a photobleaching effect [96], which results in a significant reduction in the light absorption capacity of graphene. Therefore, through the photobleaching effect, a pump light with a relatively high photon energy (short wavelength) could be used to modulate the absorption of a signal light with a relatively low photon energy [97].

Immediately following optical injection, at a timescale of tens of femtoseconds [98], the population of carriers evolves through electron–electron scattering [96] into a hot-carrier distribution [99] along the Dirac cone, resulting in an increased electronic temperature higher than the lattice temperature. In materials with strong electron–electron interactions, photoexcitation can even trigger a cascade of multiple electron–hole generation processes [100]. Subsequently, the non-equilibrium carrier distribution is broadened by the intrinsic carrier population via carrier–carrier scattering to form a hot Fermi-Dirac distribution. This ultrafast scattering process lasts for only tens to hundreds of femtoseconds [101]. The thermalized carriers are further cooled through the intraband carrier–phonon scattering [102], which occurs in a time scale of less than one picosecond. Beyond ~1 ps, electron–hole recombination becomes the dominant process, and energy could be transferred to the lattice through scattering with phonons. The equilibrium of the electronic temperature with the surrounding environment could be achieved via phonon–phonon scattering and electron-lattice cooling (dominated by supercollisions [103]). The overall evolution is summarized in Fig. 2. The time scale of the excitation–relaxation processes mentioned above
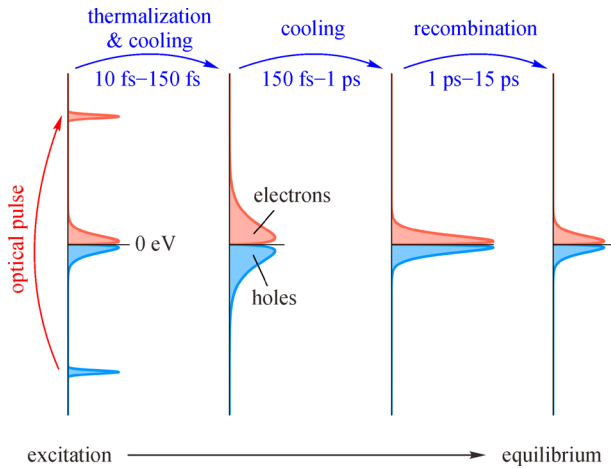
Fig. 2 Evolution of carriers in graphene from the optical excitation state to the equilibrium state. Reproduced from Ref. [108]

actually depends on the system under investigation and the excitation power. Experimentally, Fermi-level-dependent ultrafast dynamics with intraband relaxation times in the 0.4–1.7 ps range were measured by optical-pump-optical-probe spectroscopy [101,104,105]. Recently, ultrafast modulation based on saturable absorption was experimentally demonstrated using a metal-plasmonic-slot-based AOM with a response time of 0.26 ps [1]. These results indicated that the all-optical modulation speed could theoretically reach terabit(s) per second.

A hot electron model [106] showed that changes in hot electron temperature could modify the nonlinear absorption of graphene [99]. For ultrafast excitations, i.e., at bandwidths over the THz level, the temperature of the electron could be as high as 10^3 K [99], and the corresponding saturation threshold and insertion loss of the AOM could increase nonlinearly, which would deteriorate the performance of the AOM. The quality of graphene is one of the main factors that has an inevitable impact on the performances of AOMs. Poor-quality graphene is associated with lattice defects [107] and impurities, which could deteriorate its conductivity and enhance its scattering loss. The scattering coefficient of graphene is also a key factor determining its absorption [97]. Defects lead to increased absorption and, consequently, increased insertion loss for AOMs.

3 All-optical modulation with graphene

As discussed in the previous section, graphene has been identified as an auspicious material, and mesoscopic to nanoscopic structures integrated with graphene have been developed to achieve high-performance all-optical modulation. The key performance metrics [2] for graphene-based AOMs include energy consumption, response time,

modulation depth, insertion loss, and device footprint. Among them, energy consumption is particularly important for specific applications, such as in interconnects and optical computation chips. Usually, the lowest pump power required to support the modulator working at or above a certain modulation depth is called the threshold power. Therefore, the lowest energy utilized in a single bit for the pump light corresponds to the energy consumption, which is in Joule per bit (J/bit). The response time is related to the modulation speed, which determines the final bandwidth of the all-optical modulation. Modulation depth characterizes the modulator's capability to change the amplitude of the signal light. Insertion loss also plays an important role. A relatively low loss can help reduce the pump power required to generate a nonlinear effect in the modulator and ensure that signals with adequate energy are transmitted through the device to be detected by the receiver. The footprint of the device is related to the power consumption because a small size induces strong light–matter interaction with less threshold power. Based on the different configurations for launching the pump and probe light, graphene-based AOMs could be categorized into free-space modulators, fiber-based modulators, and integrated modulators. Here, we summarize the latest progress.

3.1 Free-space all-optical modulation

Free-space graphene-based AOMs can be fabricated by depositing graphene on top of planar substrates or photonic nanostructures, after which the pump and probe light is launched perpendicular to the devices. For instance, the attenuation of the THz range light wave could be achieved by the deposition of graphene on silicon (GOS), as depicted in Fig. 3(a) [89]. Photon-induced electron–hole pairs were produced in the illuminated area of silicon, and the charge could be transferred to graphene, thereby changing the conductivity of both graphene and silicon. Since the mobility of graphene is much higher than that of silicon, the absorption of the THz wave could be enhanced tremendously. In this work, light waves with frequencies from 0.2 to 2 THz could be attenuated by a 780 nm pulsed light. A modulation depth of 70% with a modulation power of 40 mW was reached, as shown in Fig. 3(b). With a relatively high modulation power, the enhancement decreased due to the charge-carrier saturation. In 2014, Wen et al. developed an all-optical terahertz modulator based on monolayer graphene deposited on germanium (GOG), which could be modulated by a 1.55 μm laser with a low photodoping power [90]. With the same operation principle, the modulation of the THz wave is achieved with a frequency ranging from 0.25 to 1 THz. A dynamic modulation measurement setup is depicted in Fig. 3(c), which uses a continuous wave source with a frequency of 0.34 THz and a 1550 nm pumping laser. At a modulation bandwidth of 20 kHz, a modulation depth of 94% can be achieved. However, the modulation depth decreased
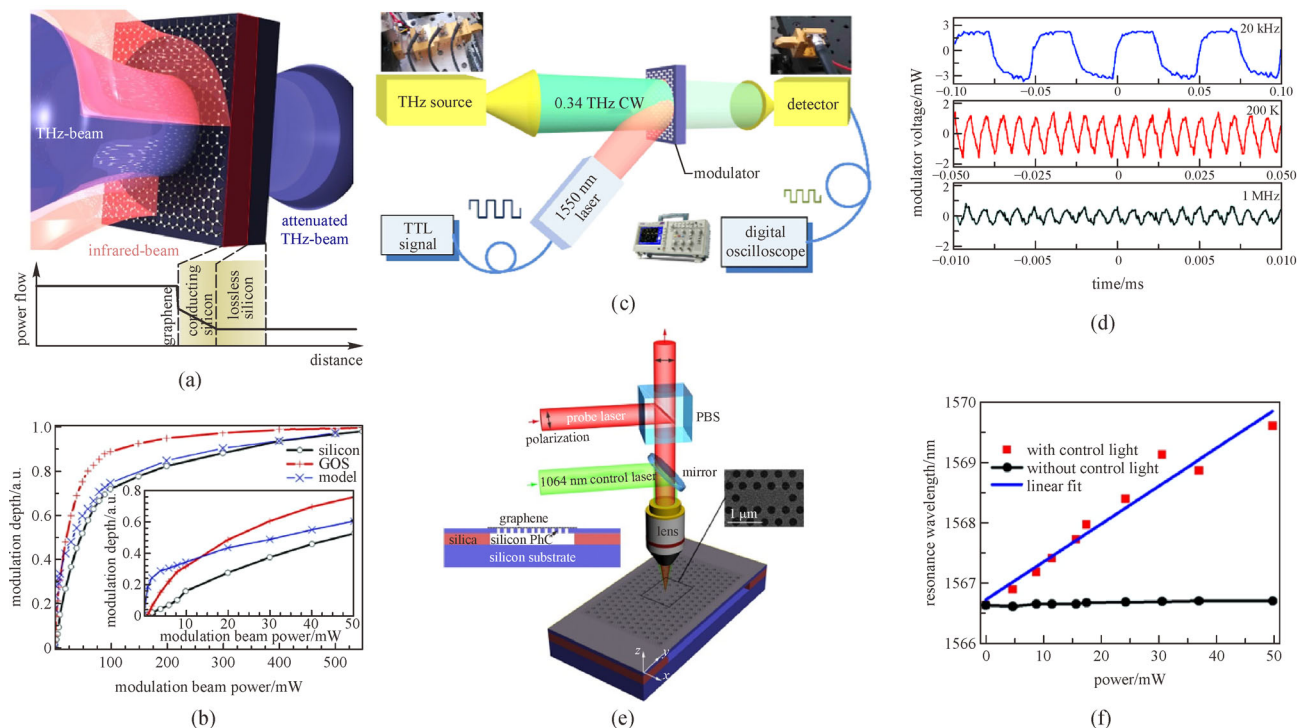
Fig. 3 (a) Illustration of the structure and modulation configuration of the graphene on silicon (GOS) AOM. The inset at the bottom illustrates the spatial dependence of the THz beam power along with the device when the modulation beam is switched on. (b) Modulation depth versus signal power of the GOS modulator. (c) Schematic of the experimental configuration used for the modulation measurements of the graphene on germanium (GOG) AOM. (d) Modulated THz signal under different modulation frequencies of the GOG modulator. (e) Experimental setup and scanning electron microscopy (SEM) image of a graphene-cladding silicon photonic crystal cavity modulator. The probe light is a narrow-band tunable semiconductor laser with a wavelength around 1550 nm, and the control laser is a 1064 nm laser. (f) Resonance wavelength variation with the control laser power of the modulator in (e). Reproduced from Refs. [89,90,113]

rapidly when the modulation rate was above 200 kHz, as shown in Fig. 3(d).

Although single-layered graphene on semiconductor could attenuate the intensity of the THz wave over 99%, light could pass through graphene only once for the free-space configuration, which resulted in a weak light–matter interaction in the visible and infrared region. The resonant structures [109] and meta-surface structures [110,111] utilized in electro-optical modulation were also employed in their all-optical counterpart [112] to further boost the modulation efficiency. In 2015, Shi et al. fabricated a graphene-cladded photonic crystal AOM [113], as shown in Fig. 3(e), which exhibited a saturable absorption threshold as low as 10 kW/cm². The ultralow threshold was attributed to the optically induced transparency (OIT), free-carrier absorption (FCA), and free-carrier dispersion effects induced by the 1064 nm pump light. The electrons in graphene excited by the pump light would be transferred into silicon, which would decrease the Fermi level of graphene, inducing the Pauli blocking effect in the probe light at a wavelength of 1550 nm. This could result in a decrease in the absorption loss inside the cavity and, thus, change the coupling condition. Moreover, the carrier injected into the silicon from graphene could further

induce the FCA and the plasma dispersion effect. With the index change of silicon, the resonant peak could shift to as high as 3.5 nm under a very low pump power input, as shown in Fig. 3(f). However, the long response time and high total energy consumption limit its applications. To solve this issue, a novel photonic platform should be introduced to enhance the interaction between light and graphene.

3.2 Fiber-based all-optical modulation

The traveling wave interaction approach could directly increase the interaction strength. In the fiber-based platform, the control light can be absorbed by graphene along its propagation path, which largely enhances the graphene–light interaction via the evanescent field of the microfiber. In 2013, Liu et al. developed an AOM by covering the 8-μm-diameter microfiber surface with 16-μm-long polydimethylsiloxane-supported graphene on a low refractive index MgF_2 substrate, as depicted in Fig. 4(a) [114]. The modulation wavelength range was 50 nm wide, the maximum modulation depth was 13 dB, and the insertion loss was 15 dB. The laser power of the pump source was 2.2 W. The interface between graphene
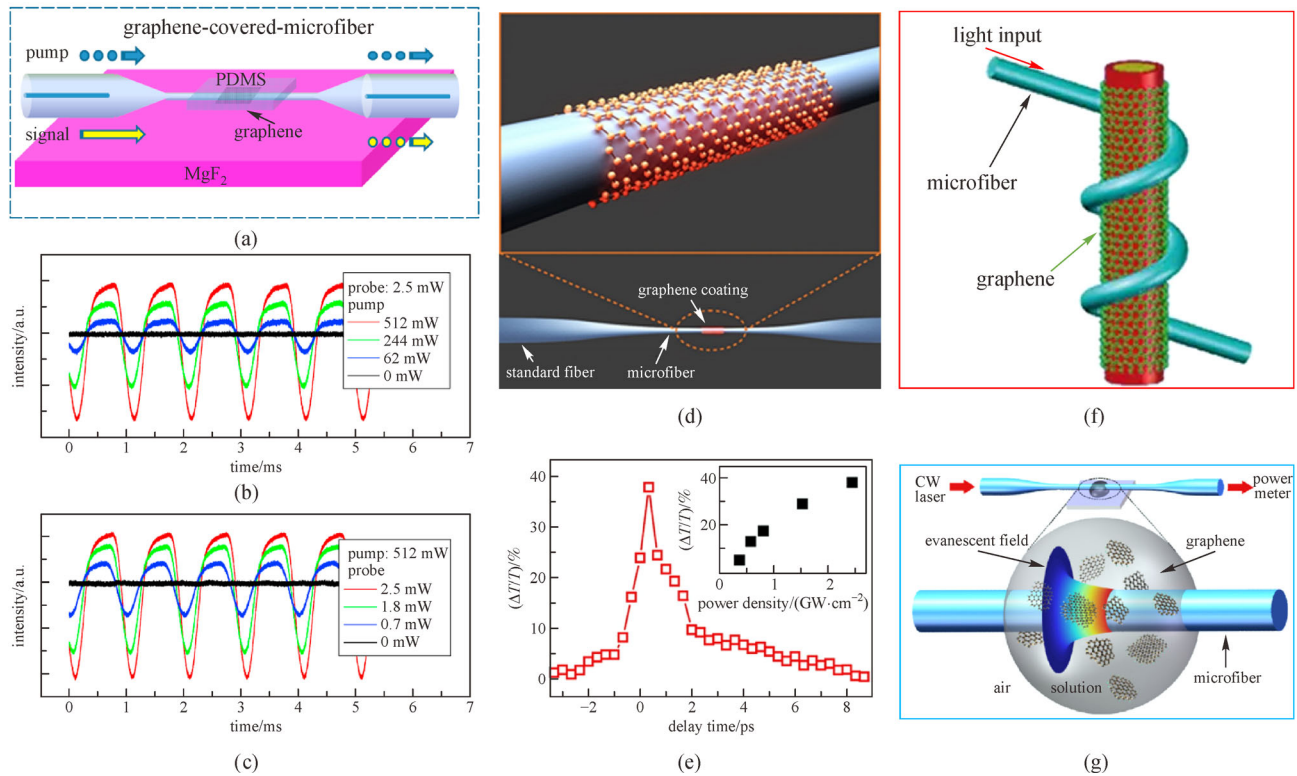
Fig. 4 (a) Schematic illustration or microscope image of broadband all-optical modulation using a PDMS-supported-graphene/ microfiber/MgF₂ structure. Intensity variations of the probe signal with the input pump power when (b) the input probe power is fixed at 2.5 mW and (c) the input pump power is fixed at 512 mW. (d) Schematic illustration of the GCM. (e) Differential transmittance of the probe light as a function of the pump–probe time delay showing a response time of approximately 2.2 ps. The inset shows the dependence of the modulation depth on the pump intensity. Schematic diagram of (f) the stereo graphene–microfiber structure, where graphene was first wrapped on a rod followed by the microfiber; (g) the graphene-decorated microfiber with a pile of graphene flakes in the surrounding space and the evanescent field. Reproduced from Refs. [104,114–116]

and the fiber was indeed overly small in such an incomplete fiber-covering configuration that the interaction was not adequate. Moreover, the power required for the pump and probe light to achieve a high modulation depth was high, as shown in Figs. 4 (b) and 4(c). A representative work was reported in 2014 by Li et al. [104] The ultrafast AOM based on a double-layer graphene-cladded micro-fiber (GCM) was introduced, as shown in Fig. 4(d). Without the carrier generation and transfer process to the semiconductor substrate, the ultrafast nature of graphene could be preserved. The relaxation time of the saturable absorption of graphene was approximately 2.2 ps, measured using the pump–probe setup, shown in Fig. 4(e), indicating a modulation bandwidth close to 200 GHz. The threshold power density in the fiber was 0.2 GW/cm², and the modulation depth reached 38%.

To further increase the interaction length, an all-optical fiber modulator based on a stereo graphene–microfiber structure (GMF) was proposed by Chen et al. [115]. As illustrated in Fig. 4(f), the microfiber was wrapped onto a graphene-coated rod, achieving a modulation depth of 7.5 dB (2.5 dB) and a modulation efficiency of 0.2 dB/W

(0.07 dB/W) for both polarizations. The limitation of the modulation depth was mainly determined by the loss resulted from the intrinsic absorption. Yu et al. demon-strated ultrafast optical modulation using a single 1-μm-diameter graphene-decorated microfiber. Benefiting from the strong evanescent wave outside the waveguide core due to the considerably small waveguide, light could actively interact with piled graphene flakes in a droplet, as shown in Fig. 4(g). The response time for the AOMs was 2.5 ps with a threshold power of 1.75 W (60 MW/cm²) [116]. In another work, the same group incorporated graphene into a fiber core using drawn graphene-polymer microfiber, and the saturable absorption threshold could be less than 0.25 pJ per pulse [117].

Apart from the saturable absorption, the thermal effect and Kerr effect had also been applied for fiber-based graphene all-optical modulation. The phase modulation induced by the two effects could be measured from fiber-based interferometric and resonant structures. In 2015, Gan et al. demonstrated a graphene-assisted all-fiber phase shifter and MZI switch by photothermal effect [84], as shown in Fig. 5(a). The heat generation from light

absorbed by graphene increased the local temperature of the graphene-covered microfiber. The optical-induced thermo-optic effect changed the refractive index of the microfiber, and the phase shift modulated the intensity of the light output from the MZI switch. The modulation depth could be as high as 20 dB. The phase shift energy efficiency was 0.09 π/mW, while the fall time was around 3.2 ms. To further boost the energy efficiency and modulation speed, microfiber resonators with wrapped graphene have been fabricated, and light could be circulating inside the ring to enhance the absorption by graphene [85], as illustrated in Fig. 5(b). Thus, the all-optical switch could achieve a 71 pm/mW resonance peak wavelength shift efficiency and a modulation depth of 13 dB with a response speed with a rising (fall) time of 294.7 μs (212.2 μs). However, the thermal response time was slow, and the ultrafast phase modulation could only be achieved by the Kerr effect. As shown in Fig. 5(c), a GCM structure was inserted into an MZI with variable internal attenuators to fine-tune the output transmission [92]. Using a fiber-based wavelength division multiplexer, 1064 nm nanosecond pulses were injected as switching light. With a peak power of 1.18 W, the phase modulation could be as high as 0.18 π, with a response time of < 10 ns due to the optical Kerr effect.

Besides the microfibers, side-polished D-shape fibers have also been used in graphene-based AOMs. In 2016, Zhang et al. [118] fabricated an in-fiber optical modulator developed on a side-polished optical fiber (shown in

Fig. 5(d)). By polishing the fiber to an ultra-smooth surface (roughness < 1 nm), scattering from the interface was minimized, and consequently, low insertion loss (< 1 dB) could be achieved. To enhance the light–matter interaction, the graphene film was coated with a high index polyvinyl butyral (PVB) layer so that the light field could be drawn closer to graphene. Using this innovative approach, an extinction ratio of 9 dB and response time less than 1 ps were realized. Debnath et al. [119] demonstrated a similar structure, as depicted in Fig. 5(e). All-optical switching near 1550 nm was elucidated by exploiting FWM with in situ grown graphene. The incident signal was modulated at a speed of up to 20 GHz, and the modulation information was successfully transferred to the generated signals at different wavelengths.

During the past 10 years, fiber-based AOMs have made great progress with modulation depths over 99% and response times around 2 ps with a low switching threshold. However, the microfiber system is fragile, and the fabrication process for D-shaped fiber is nontrivial. It is difficult to build a complex photonic network based on the fiber platform via large-scale integration. The integrated graphene all-optical switches discussed in the next subsection could be the potential solution to this challenge.

3.3 On-chip all-optical modulation

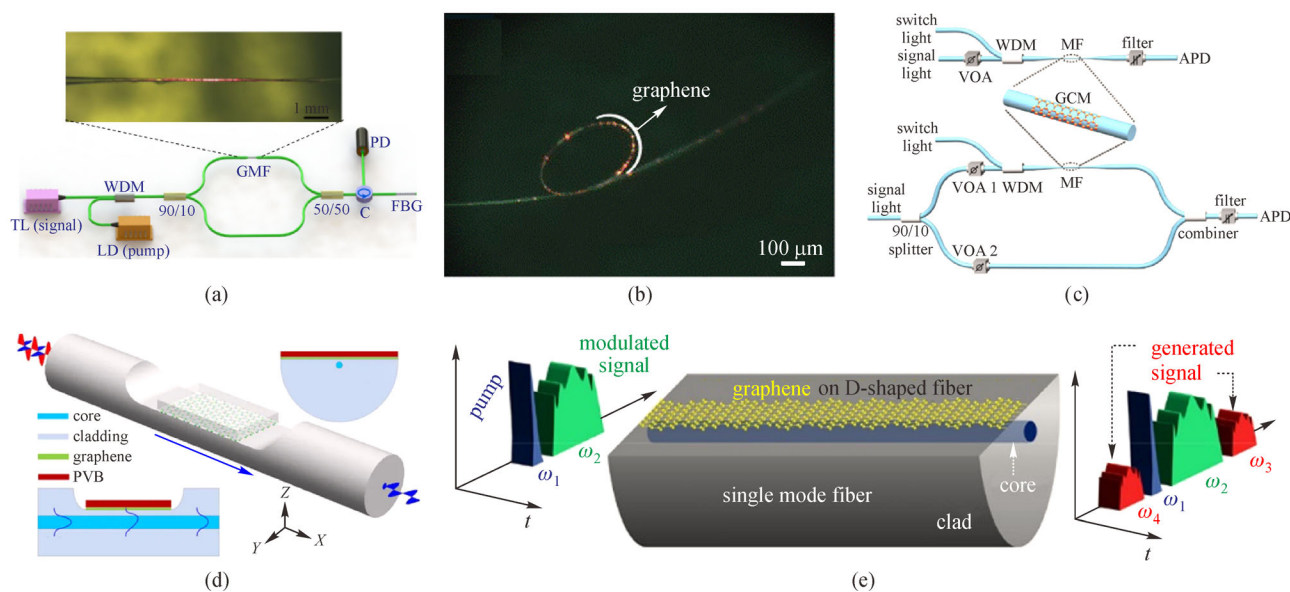To further enhance the light–matter interaction, integrated graphene with a high index contrast planar photonic

Fig. 5 (a) Optical microscopic image of the tapered graphene-coated microfiber and schematic of the measurement setup. (b) Microscope image of graphene on the microfiber resonator and the graphene-coated region is annotated by the white curve. (c) Schematic diagram of GCM-based AOMs based on an all-fiber MZI. (d) Schematic and cross-sectional view of the polyvinyl butyral (PVB)-covered graphene on a partly-polished fiber AOM. The longitudinal cross-section shows detailed layers of the device. (e) Structural diagram of the as-grown graphene on a D-shaped fiber, and the FWM process shows two newly generated signals (ω_3 and ω_4). Reproduced from Refs. [84,85,92,118,119]

structure [120] could be a favorable solution. To the best of our knowledge, the earliest on-chip device was reported in 2014. Local and nonlocal OIT effects (slightly different from the OIT effect mentioned in Subsection 3.1) in graphene on silica/silicon hybrid photonic integrated circuits [121] were demonstrated, as shown in Fig. 6(a). The probe light was coupled into the circuit by a grating coupler, while the pump light was vertically illuminating onto the 100-μm-long interaction zone, exciting the carriers in silicon. Subsequently, the excited carriers are transferred to graphene, causing its Fermi level to shift. The power required for producing the OIT effect is as low as 0.1 mW for a continuous wave of light. The corresponding power density is 2 W/cm², while the modulation rate is in the Hz level, as depicted in Fig. 6(b). The power–speed trade-off is clearly reflected. Such an in-direct interaction between the signal light and graphene results in a low modulation speed.

In 2017, Qiu et al. [86] realized all-optical control on a graphene-on-Si_3N_4 chip based on the photothermal effect. Graphene was integrated with the ring resonator, as depicted in Fig. 6(c), with a length of 43.4 μm. The heat generated from the graphene by absorption of the pump light changed the refractive index of the Si_3N_4 waveguide and induced the shifting of the resonant wavelength. A switching response time of 253.0 ns (rise time of the modulated signal, Fig. 6(d)) with a switching energy of ~50 nJ was obtained, demonstrating a modulation depth of 10 dB. However, the response time is still lower than those of state-of-the-art fiber-based all-optical switches [104].

To take advantage of the ultrafast response of graphene, the saturable absorption effect should play a major role. The AOM based on the Pauli blocking effect in a dielectric-loaded waveguide (DLW) with a graphene–silicon heterojunction structure (GSH) is shown in Fig. 6(e) [122]. The DLW–GSH structure supports a TM mode, where the maximum electric field intensity locates at the bottom of the waveguide, where the graphene is positioned, facilitating a strong light–graphene interaction. Under the modulation light with a wavelength of 532 nm and a power of 60 mW, a modulation efficiency of 0.0275 dB/μm was achieved, as illustrated in Fig. 6(f). To further increase the interaction strength, an AOM based on a graphene–plasmonic slot-waveguide structure was developed [123], as shown in Fig. 6(g). The length of the graphene–plasmonic slot-waveguide device was 10 μm. The modulation efficiency was enhanced by the strong interaction between the light and the graphene–plasmonic structure because of the high local-field distribution. Even though the modulation speed was not mentioned either, a modulation efficiency of 0.21 dB/μm was obtained, as plotted in Fig. 6(h). In these two examples, the interaction between the pump light and graphene is achieved by free-space illuminated on top of the devices. To further improve the pump efficiency, it is necessary to also couple the pump light in the plane along with the photonic structure.

Recently, an AOM based on the graphene–silicon hybrid waveguides with a graphene length of 30 μm was demonstrated [124]. A modulation depth of 22.7% was achieved with the saturation threshold lowered to 1.38 pJ
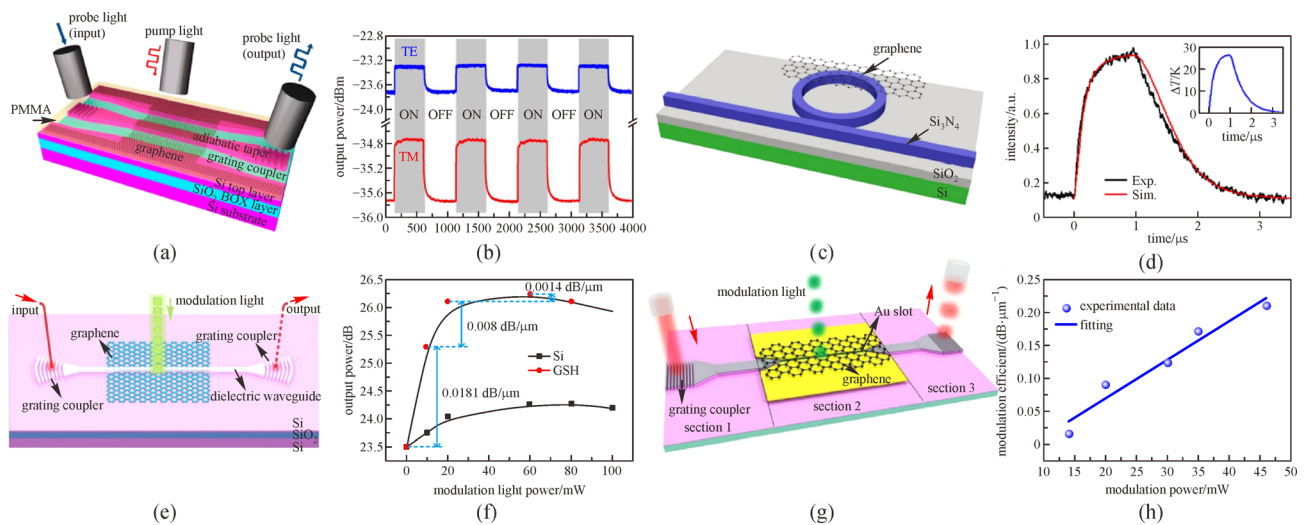

Fig. 6 (a) Three-dimensional schematic illustration of a graphene/silicon/silica hybrid nanophotonic waveguide. The probe light is coupled using grating couplers, and the pump light is emitted from the top of the sample. (b) Dynamic responses of the output power for the TE and TM modes of hybrid nanophotonic wires with a local pump light. (c) Schematic diagram of the graphene-on-Si_3N_4 all-optical device. (d) Temporal response of the output probe pulse. Inset: average temperature change. (e) Schematic illustration of the graphene–silicon heterojunction modulator with the signal coupled by grating couplers and pump light illuminating from the free space. (f) Comparative performance of GSH and pure silicon AOMs at different modulation laser powers. (g) Schematic illustration of the graphene–plasmonic slot-waveguide AOM. (h) Modulation efficiency with respect to the modulation power. Reproduced from Refs. [86,121–123]

per pulse, and a response time of 1.65 ps. In 2019, a device similar to the one in Ref. [123] with graphene-loaded ultra-compact plasmonic slot waveguides was reported by Masaya Notomi's group [1]. The all-optical plasmonic slot switch had a relatively small interaction volume and exhibited more significant confinement of the light propagating in graphene. Ultrafast and energy-efficient all-optical switches have been realized since the traditional trade-off between energy consumption and the modulation speed has been overcome. First, deep subwavelength plasmonic waveguides with a mode volume of only 30 nm × 20 nm were used to provide extreme light confinement, and therefore, greatly enhanced nonlinear absorption in graphene was achieved. Secondly, two ultralow-loss mode

converters [125] were applied to minimize the insertion loss between the silicon waveguide and the plasmonic waveguide, as depicted in Fig. 7(a), which guaranteed a high pump light coupling efficiency. Thirdly, both the pump and probe light were coupled from the silicon waveguide to the interaction region with a length of fewer than 10 μm, and the traveling wave configuration was not perturbed by the photon lifetime of the cavity structure. Moreover, the ultrafast carrier diffusion out of the 30-nm-wide slot region [126] guaranteed the ultrashort response time, which is even shorter than the relation time of excitons in graphene. With a modulation depth of 3.5 dB, ultrafast all-optical switching with a switching energy of 35 fJ and a switching time of 0.26 ps was achieved, as
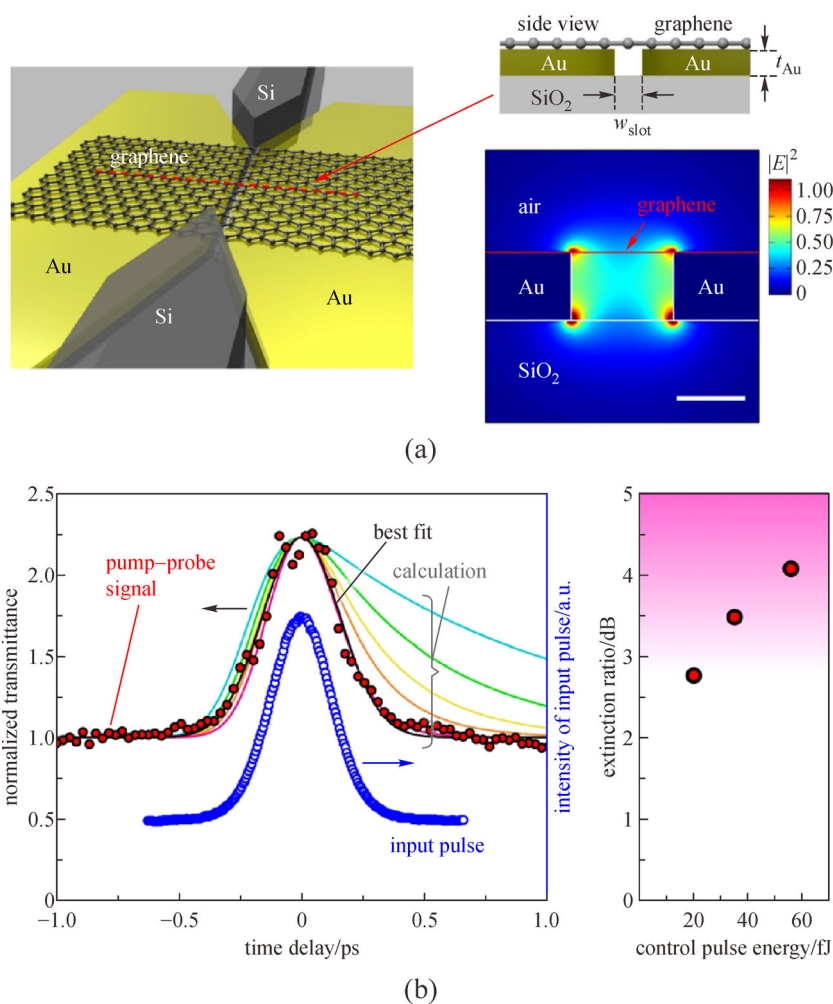

(a)

(b)

Fig. 7 (a) Schematic of the graphene-loaded metal–insulator–metal (MIM)-waveguide (WG). Cross-sectional side view of the MIM-WG. Calculated field profile of the eigenmode of the graphene-loaded MIM-WG. The air slot width (w_{slot}) is 30 nm, and the Au thickness (t_{Au}) is 20 nm. The scale bar is 20 nm. (b) Left: results of the pump–probe measurement. (Red circles) All-optical switching in the bilayer-graphene-loaded MIM-WG. (Blue circles) The autocorrelation of the input pulse. The input pulse width was 210 fs. (Solid black line) The Gaussian fit of the pump–probe signal. The control and signal pulse energies were 35 and 1.3 fJ, respectively, in the input silicon-wire WG. The pump–probe signals predicted from t_{pulse} (210 fs) and the relaxation time of the graphene carrier, τ, are also shown, where two Gaussian functions (FWHM = 210 fs) and a single exponential decay function (τ from 100 fs to 1 ps) are convoluted. The magenta, orange-yellow, green, and light blue lines are for τ = 100 fs, 200 fs, 300 fs, 500 fs, and 1 ps, respectively. Right: control pulse energy dependence of the extinction ratio for the bilayer-graphene-loaded MIM-WG. Reproduced from Ref. [1]

Table 1 Performance matrix of the state-of-the-art graphene-based AOMs

structure	principle	Rt/MF	MD	PC/TPD	Ref.
Gra/Ge subsrate	carrier induced $\Delta\kappa$	200 kHz	94%	400 mW	[90]
Gra/silicon PhC	saturable absorption, carrier induced Δn	–	–	10 kW/cm^2	[113]
Gra/fiber	saturable absorption	2.2 ps	38%	0.2 GW/cm^2	[104]
Gra/fiber MZI	Kerr	10 ns	52%	52.5 μW	[92]
Gra/fiber knot	thermal	294.7 μs	13 dB	2.6 mW	[85]
Gra/Si$_3$N$_4$/SiO$_2$	thermal	253 ns	10 dB	50 nJ	[86]
Gra/SOI	saturable absorption	1.65 ps	22.7%	1.38 pJ	[124]
105Gra/MIM slot	saturable absorption	0.26 ps	3.5 dB	35 fJ	[1]

exhibited in Fig. 7(b). The switching energy is a new record in graphene-based devices and all-optical switch operating at a few picoseconds or less. In addition, the compatibility with existing silicon photonic technologies reveals the great application potential of the graphene-based deep subwavelength metal–insulator–metal all-optical switch in the next generation ultrafast and ultralow power photonic networks on-a-chip.

4   Discussion and outlook

All-optical signal processing is an indispensable part of optical interconnection systems. Developing small, fast, and energy-efficient AOMs has been and will be an everlasting goal of the research community. For practical applications, superior performance is always favored, and graphene, with an intrinsic ultrashort relaxation time and high nonlinearity, could well satisfy this need. In this review, we discussed the substantial progress in the performance of graphene-based AOMs, and the performance matrix for the state-of-the-art devices is listed in Table 1, where Rt, MF, MD, PC, TPD, Ref., and Gra refer to the response time, modulation frequency, modulation depth, power consumption, threshold power density, reference number, and graphene, respectively.

The free-space approach and the fiber-based approach are highly suitable for the fabrication process. The light–matter interaction in the free-space pumping AOM is quite weak; therefore, the applications are limited. In the microfiber platform, the interaction, which occurs on the surface of the microfiber, could significantly enhance the interaction with graphene at a low power threshold [127] with an ultrafast response time (lowered to picoseconds). However, the power density required in the microfiber is still high. Due to the strong light confinement requirement for the on-chip AOMs, their size and energy consumptions were typically considerably low. To date, the graphene-based AOM has delivered the best performance among AOMs, presenting the smallest power threshold and fastest

relaxation process. The on-chip strategy shows remarkable advantages and plays an irreplaceable role in the AOM research field.

Although significant progress has been made in the graphene-based AOM field in the past few years, some challenges still exist. The first is related to the method of obtaining high-quality and new graphene-based heterostructure nonlinear materials with relatively fast response times and large optical nonlinearity. The second is related to the method of integrating novel structures with CMOS compatibility with the single layer of graphene to enhance light interaction. The third challenge is that graphene-based all-optic logic devices with reconfigurability have not been developed yet. Encouragingly, these challenges help establish future research directions. The first research direction is centered on the exploration of novel 2D materials and their heterostructures with graphene to achieve high-performance nonlinear optical van-der Waals materials. Apart from graphene, other 2D materials such as black phosphorus (BP) [128] and 2D transition metal dichalcogenides (TMDs) [28] with unique spectral responses are also attractive frontiers for achieving high-performance AOMs. Moreover, these novel 2D materials could be combined with graphene with different stacking angles, band structures, and layer numbers, which would probably offer new mechanisms and configurations for all-optical modulation. The second research direction is aimed toward the development of a CMOS-compatible metallic plasmonic structure [123,129,130] for large-scale photonic integration. Thirdly, graphene-based all-optical process integrated photonic circuits with cascaded reconfigurable nanoscale switches would be greatly instrumental in complicated logic processing circuits, ultra-high bandwidth photonic interconnect on-a-chip, and quantum photonic networks.

References

1. Ono M, Hata M, Tsunekawa M, Nozaki K, Sumikura H, Chiba H, Notomi M. Ultrafast and energy-efficient all-optical switching with graphene-loaded deep-subwavelength plasmonic waveguides. Nature Photonics, 2020, 14(1): 37–43

2. Reed G T, Mashanovich G, Gardes F Y, Thomson D J. Silicon optical modulators. Nature Photonics, 2010, 4(8): 518–526

3. He M, Xu M, Ren Y, Jian J, Ruan Z, Xu Y, Gao S, Sun S, Wen X, Zhou L, Liu L, Guo C, Chen H, Yu S, Liu L, Cai X. High-performance hybrid silicon and lithium niobate Mach–Zehnder modulators for 100 Gbit·s^{-1} and beyond. Nature Photonics, 2019, 13(5): 359–364

4. Wang C, Zhang M, Chen X, Bertrand M, Shams-Ansari A, Chandrasekhar S, Winzer P, Lončar M. Integrated lithium niobate electro-optic modulators operating at CMOS-compatible voltages. Nature, 2018, 562(7725): 101–104

5. Li M, Wang L, Li X, Xiao X, Yu S. Silicon intensity Mach–Zehnder modulator for single lane 100 Gb/s applications. Photonics Research, 2018, 6(2): 109–116

6. Alloatti L, Palmer R, Diebold S, Pahl K P, Chen B, Dinu R, Fournier M, Fedeli J M, Zwick T, Freude W, Koos C, Leuthold J. 100 GHz silicon–organic hybrid modulator. Light, Science & Applications, 2014, 3(5): e173

7. Haffner C, Heni W, Fedoryshyn Y, Niegemann J, Melikyan A, Elder D L, Baeuerle B, Salamin Y, Josten A, Koch U, Hoessbacher C, Ducry F, Juchli L, Emboras A, Hillerkuss D, Kohl M, Dalton L R, Hafner C, Leuthold J. All-plasmonic Mach–Zehnder modulator enabling optical high-speed communication at the microscale. Nature Photonics, 2015, 9(8): 525–528

8. Ayata M, Fedoryshyn Y, Heni W, Baeuerle B, Josten A, Zahner M, Koch U, Salamin Y, Hoessbacher C, Haffner C, Elder D L, Dalton L R, Leuthold J. High-speed plasmonic modulator in a single metal layer. Science, 2017, 358(6363): 630–632

9. Haffner C, Chelladurai D, Fedoryshyn Y, Josten A, Baeuerle B, Heni W, Watanabe T, Cui T, Cheng B, Saha S, Elder D L, Dalton L R, Boltasseva A, Shalaev V M, Kinsey N, Leuthold J. Low-loss plasmon-assisted electro-optic modulator. Nature, 2018, 556 (7702): 483–486

10. Davoodi F, Granpayeh N. All optical logic gates – a tutorial. International Journal of Information & Communication Technology Research, 2012, 43(3): 65–98

11. Singh P, Tripathi D K, Jaiswal S, Dixit H K. All-optical logic gates: designs, classification, and comparison. Advances in Optical Technologies, 2014, 2014: 275083

12. Minzioni P, Lacava C, Tanabe T, Dong J, Hu X, Csaba G, Porod W, Singh G, Willner A E, Almaiman A, Torres-Company V, Schröder J, Peacock A C, Strain M J, Parmigiani F, Contestabile G, Marpaung D, Liu Z, Bowers J E, Chang L, Fabbri S, Ramos Vázquez M, Bharadwaj V, Eaton S M, Lodahl P, Zhang X, Eggleton B J, Munro W J, Nemoto K, Morin O, Laurat J, Nunn J. Roadmap on all-optical processing. Journal of Optics, 2019, 21(6): 063001

13. Chai Z, Hu X, Wang F, Niu X, Xie J, Gong Q. Ultrafast all-optical switching. Advanced Optical Materials, 2017, 5(7): 1600665

14. Sasikala V, Chitra K. All optical switching and associated technologies: a review. Journal of Optics, 2018, 47(3): 307–317

15. Almeida V R, Barrios C A, Panepucci R R, Lipson M. All-optical control of light on a silicon chip. Nature, 2004, 431(7012): 1081–1084

16. Koos C, Vorreau P, Vallaitis T, Dumon P, Bogaerts W, Baets R, Esembeson B, Biaggio I, Michinobu T, Diederich F, Freude W, Leuthold J. All-optical high-speed signal processing with silicon–organic hybrid slot waveguides. Nature Photonics, 2009, 3(4): 216–219

17. Gholipour B, Zhang J, MacDonald K F, Hewak D W, Zheludev N I. An all-optical, non-volatile, bidirectional, phase-change meta-switch. Advanced Materials, 2013, 25(22): 3050–3054

18. Chai Z, Zhu Y, Hu X, Yang X, Gong Z, Wang F, Yang H, Gong Q. On-chip optical switch based on plasmon-photon hybrid nanostructure-coated multicomponent nanocomposite. Advanced Optical Materials, 2016, 4(8): 1159–1166

19. Nozaki K, Tanabe T, Shinya A, Matsuo S, Sato T, Taniyama H, Notomi M. Sub-femtojoule all-optical switching using a photonic-crystal nanocavity. Nature Photonics, 2010, 4(7): 477–483

20. Vo T D, Pant R, Pelusi M D, Schröder J, Choi D Y, Debbarma S K, Madden S J, Luther-Davies B, Eggleton B J. Photonic chip-based all-optical XOR gate for 40 and 160 Gbit/s DPSK signals. Optics Letters, 2011, 36(5): 710–712

21. Hou J, Chen L, Dong W, Zhang X. 40 Gb/s reconfigurable optical logic gates based on FWM in silicon waveguide. Optics Express, 2016, 24(3): 2701–2711

22. Chai Z, Zhu Y, Hu X Y, Yang X Y, Gong Z B, Wang F F, Yang H, Gong Q H. On-chip optical switch based on plasmon-photon hybrid nanostructure-coated multicomponent nanocomposite. Advanced Optical Materials, 2016, 4(8): 1159–1166

23. Wang F, Hu X, Song H, Li C, Yang H, Gong Q. Ultralow-power all-optical logic data distributor based on resonant excitation enhanced nonlinearity by upconversion radiative transfer. Advanced Optical Materials, 2017, 5(20): 1700360

24. Chai Z, Hu X, Wang F, Li C, Ao Y, Wu Y, Shi K, Yang H, Gong Q. Ultrafast on-chip remotely-triggered all-optical switching based on epsilon-near-zero nanocomposites. Laser & Photonics Reviews, 2017, 11(5): 1700042

25. Yang X, Hu X, Yang H, Gong Q. Ultracompact all-optical logic gates based on nonlinear plasmonic nanocavities. Nanophotonics, 2017, 6(1): 365–376

26. Dong W, Huang Z, Hou J, Santos R, Zhang X. Integrated all-optical programmable logic array based on semiconductor optical amplifiers. Optics Letters, 2018, 43(9): 2150–2153

27. Guo B, Xiao Q L, Wang S H, Zhang H. 2D layered materials: synthesis, nonlinear optical properties, and device applications. Laser & Photonics Reviews, 2019, 13(12): 1800327

28. Manzeli S, Ovchinnikov D, Pasquier D, Yazyev O V, Kis A. 2D transition metal dichalcogenides. Nature Reviews. Materials, 2017, 2(8): 17033

29. Tarruell L, Greif D, Uehlinger T, Jotzu G, Esslinger T. Creating, moving and merging Dirac points with a Fermi gas in a tunable honeycomb lattice. Nature, 2012, 483(7389): 302–305

30. Xia F, Wang H, Xiao D, Dubey M, Ramasubramaniam A. Two-dimensional material nanophotonics. Nature Photonics, 2014, 8 (12): 899–907

31. Yu S, Wu X, Wang Y, Guo X, Tong L. 2D materials for optical modulation: challenges and opportunities. Advanced Materials, 2017, 29(14): 1606128

32. Jin L, Ma X, Zhang H, Zhang H, Chen H, Xu Y. 3 GHz passively harmonic mode-locked Er-doped fiber laser by evanescent field-based nano-sheets topological insulator. Optics Express, 2018, 26(24): 31244–31252

33. Koo J, Park J, Lee J, Jhon Y M, Lee J H. Femtosecond harmonic mode-locking of a fiber laser at 3.27 GHz using a bulk-like, $MoSe_2$-based saturable absorber. Optics Express, 2016, 24(10): 10575–10589

34. Li Z, Li R, Pang C, Dong N, Wang J, Yu H, Chen F. 8.8 GHz Q-switched mode-locked waveguide lasers modulated by $PtSe_2$ saturable absorber. Optics Express, 2019, 27(6): 8727–8737

35. Liu M, Tang R, Luo A P, Xu W C, Luo Z C. Graphene-decorated microfiber knot as a broadband resonator for ultrahigh repetition-rate pulse fiber lasers. Photonics Research, 2018, 6(10): C1–C7

36. Liu M, Zheng X W, Qi Y L, Liu H, Luo A P, Luo Z C, Xu W C, Zhao C J, Zhang H. Microfiber-based few-layer MoS_2 saturable absorber for 2.5 GHz passively harmonic mode-locked fiber laser. Optics Express, 2014, 22(19): 22841–22846

37. Liu W, Pang L, Han H, Liu M, Lei M, Fang S, Teng H, Wei Z. Tungsten disulfide saturable absorbers for 67 fs mode-locked erbium-doped fiber lasers. Optics Express, 2017, 25(3): 2950–2959

38. Qi Y L, Liu H, Cui H, Huang Y Q, Ning Q Y, Liu M, Luo Z C, Luo A P, Xu W C. Graphene-deposited microfiber photonic device for ultrahigh-repetition rate pulse generation in a fiber laser. Optics Express, 2015, 23(14): 17720–17726

39. Yan P, Lin R, Ruan S, Liu A, Chen H. A 2.95 GHz, femtosecond passive harmonic mode-locked fiber laser based on evanescent field interaction with topological insulator film. Optics Express, 2015, 23(1): 154–164

40. Luo Z, Li Y, Zhong M, Huang Y, Wan X, Peng J, Weng J. Nonlinear optical absorption of few-layer molybdenum diselenide ($MoSe_2$) for passively mode-locked soliton fiber laser. Photonics Research, 2015, 3(3): A79–A86

41. Zhang B Y, Liu T, Meng B, Li X, Liang G, Hu X, Wang Q J. Broadband high photoresponse from pure monolayer graphene photodetector. Nature Communications, 2013, 4(1): 1811

42. Tan W C, Huang L, Ng R J, Wang L, Hasan D M N, Duffin T J, Kumar K S, Nijhuis C A, Lee C, Ang K W. A black phosphorus carbide infrared phototransistor. Advanced Materials, 2018, 30(6): 1705039

43. Talebi H, Dolatyari M, Rostami G, Manzuri A, Mahmudi M, Rostami A. Fabrication of fast mid-infrared range photodetector based on hybrid graphene-PbSe nanorods. Applied Optics, 2015, 54(20): 6386–6390

44. Jabbarzadeh F, Siahsar M, Dolatyari M, Rostami G, Rostami A. Fabrication of new mid-infrared photodetectors based on graphene modified by organic molecules. IEEE Sensors Journal, 2015, 15(5): 2795–2800

45. Huang L, Tan W C, Wang L, Dong B, Lee C, Ang K W. Infrared black phosphorus phototransistor with tunable responsivity and low noise equivalent power. ACS Applied Materials & Interfaces, 2017, 9(41): 36130–36136

46. Guo Q, Pospischil A, Bhuiyan M, Jiang H, Tian H, Farmer D, Deng B, Li C, Han S J, Wang H, Xia Q, Ma T P, Mueller T, Xia F. Black phosphorus mid-infrared photodetectors with high gain. Nano Letters, 2016, 16(7): 4648–4655

47. Xia F, Wang H, Xiao D, Dubey M, Ramasubramaniam A. Two-dimensional material nanophotonics. Nature Photonics, 2014, 8(12): 899–907

48. Sun Z, Martinez A, Wang F. Optical modulators with 2D layered materials. Nature Photonics, 2016, 10(4): 227–238

49. Youngblood N, Li M. Integration of 2D materials on a silicon photonics platform for optoelectronics applications. Nanophotonics, 2017, 6(6): 1205–1218

50. Ma Z, Hemnani R, Bartels L, Agarwal R, Sorger V J. 2D materials in electro-optic modulation: energy efficiency, electrostatics, mode overlap, material transfer and integration. Applied Physics A, Materials Science & Processing, 2018, 124(2): 126

51. Fang Y, Ge Y, Wang C, Zhang H. Mid-infrared photonics using 2D materials: status and challenges. Laser & Photonics Reviews, 2020, 14(1): 1900098

52. Geim A K, Novoselov K S. The rise of graphene. Nature Materials, 2007, 6(3): 183–191

53. Bao Q, Zhang H, Ni Z, Wang Y, Polavarapu L, Shen Z, Xu Q, Tang D, Loh K P. Monolayer graphene as a saturable absorber in a mode-locked laser. Nano Research, 2011, 4(3): 297–307

54. Bao Q, Zhang H, Wang Y, Ni Z, Yan Y, Shen Z X, Loh K P, Tang D Y. Atomic-layer graphene as a saturable absorber for ultrafast pulsed lasers. Advanced Functional Materials, 2009, 19(19): 3077–3083

55. Bao Q, Zhang H, Yang J, Wang S, Tang D, Jose R, Ramakrishna S, Lim C T, Loh K P. Graphene-polymer nanofiber membrane for ultrafast photonics. Advanced Functional Materials, 2010, 20(5): 782–791

56. Zhang H, Tang D, Knize R J, Zhao L, Bao Q, Loh K P. Graphene mode locked, wavelength-tunable, dissipative soliton fiber laser. Applied Physics Letters, 2010, 96(11): 111112

57. Liu X M, Yang H R, Cui Y D, Chen G W, Yang Y, Wu X Q, Yao X K, Han D D, Han X X, Zeng C, Guo J, Li W L, Cheng G, Tong L M. Graphene-clad microfibre saturable absorber for ultrafast fibre lasers. Scientific Reports, 2016, 6(1): 26024

58. Wu J, Yang Z, Qiu C, Zhang Y, Wu Z, Yang J, Lu Y, Li J, Yang D, Hao R, Li E, Yu G, Lin S. Enhanced performance of a graphene/GaAs self-driven near-infrared photodetector with upconversion nanoparticles. Nanoscale, 2018, 10(17): 8023–8030

59. Flöry N, Ma P, Salamin Y, Emboras A, Taniguchi T, Watanabe K, Leuthold J, Novotny L. Waveguide-integrated van der Waals heterostructure photodetector at telecom wavelengths with high speed and high responsivity. Nature Nanotechnology, 2020, 15(2): 118–124

60. Wang X, Gan X. Graphene integrated photodetectors and opto-electronic devices – a review. Chinese Physics B, 2017, 26(3): 034201

61. Youngblood N, Anugrah Y, Ma R, Koester S J, Li M. Multifunctional graphene optical modulator and photodetector integrated on silicon waveguides. Nano Letters, 2014, 14(5): 2741–2746

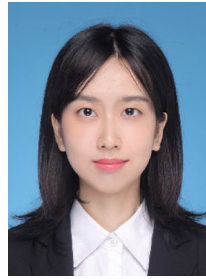62. Gao Y, Shiue R J, Gan X, Li L, Peng C, Meric I, Wang L, Szep A,

Walker D Jr, Hone J, Englund D. High-speed electro-optic modulator integrated with graphene-boron nitride heterostructure and photonic crystal nanocavity. Nano Letters, 2015, 15(3): 2001–2005

63. Liu M, Yin X, Ulin-Avila E, Geng B, Zentgraf T, Ju L, Wang F, Zhang X. A graphene-based broadband optical modulator. Nature, 2011, 474(7349): 64–67

64. Liang G, Hu X, Yu X, Shen Y, Li L H, Davies A G, Linfield E H, Liang H K, Zhang Y, Yu S F, Wang Q J. Integrated terahertz graphene modulator with 100% modulation depth. ACS Photonics, 2015, 2(11): 1559–1566

65. Phare C T, Daniel Lee Y H, Cardenas J, Lipson M. Graphene electro-optic modulator with 30 GHz bandwidth. Nature Photonics, 2015, 9(8): 511–514

66. Yu L, Yin Y, Shi Y, Dai D, He S. Thermally tunable silicon photonic microdisk resonator with transparent graphene nanoheaters. Optica, 2016, 3(2): 159–166

67. Yan S, Zhu X, Frandsen L H, Xiao S, Mortensen N A, Dong J, Ding Y. Slow-light-enhanced energy efficiency for graphene microheaters on silicon photonic crystal waveguides. Nature Communications, 2017, 8(1): 14411

68. Lin H, Song Y, Huang Y, Kita D, Deckoff-Jones S, Wang K, Li L, Li J, Zheng H, Luo Z, Wang H, Novak S, Yadav A, Huang C C, Shiue R J, Englund D, Gu T, Hewak D, Richardson K, Kong J, Hu J. Chalcogenide glass-on-graphene photonics. Nature Photonics, 2017, 11(12): 798–805

69. Wu J, Lu Y, Feng S, Wu Z, Lin S, Hao Z, Yao T, Li X, Zhu H, Lin S. The interaction between quantum dots and graphene. Applications in Graphene-Based Solar Cells and Photodetectors, 2018, 28 (50): 1804712

70. Sorianello V, Midrio M, Contestabile G, Asselberghs I, Van Campenhout J, Huyghebaert C, Goykhman I, Ott A K, Ferrari A C, Romagnoli M. Graphene–silicon phase modulators with gigahertz bandwidth. Nature Photonics, 2018, 12(1): 40–44

71. Cheng Z, Zhu X, Galili M, Frandsen L H, Hu H, Xiao S, Dong J, Ding Y, Oxenløwe L K, Zhang X. Double-layer graphene on photonic crystal waveguide electro-absorption modulator with 12 GHz bandwidth. Nanophotonics, 2019, doi: 10.1515/nanoph-2019-0381

72. Chen K, Zhou X, Cheng X, Qiao R, Cheng Y, Liu C, Xie Y, Yu W, Yao F, Sun Z, Wang F, Liu K, Liu Z. Graphene photonic crystal fibre with strong and tunable light–matter interaction. Nature Photonics, 2019, 13(11): 754–759

73. Cheng Z, Cao R, Guo J, Yao Y, Wei K, Gao S, Wang Y, Dong J, Zhang H. Phosphorene-assisted silicon photonic modulator with fast response time. Nanophotonics, 2020, doi: 10.1515/nanoph-2019-0510

74. Novoselov K S, Geim A K, Morozov S V, Jiang D, Katsnelson M I, Grigorieva I V, Dubonos S V, Firsov A A. Two-dimensional gas of massless Dirac fermions in graphene. Nature, 2005, 438(7065): 197–200

75. Geim A K. Graphene: status and prospects. Science, 2009, 324 (5934): 1530–1534

76. Luo S, Wang Y, Tong X, Wang Z. Graphene-based optical modulators. Nanoscale Research Letters, 2015, 10(1): 199

77. Bolotin K I, Sikes K J, Jiang Z, Klima M, Fudenberg G, Hone J, Kim P, Stormer H L. Ultrahigh electron mobility in suspended graphene. Solid State Communications, 2008, 146(9–10): 351–355

78. Mak K F, Sfeir M Y, Wu Y, Lui C H, Misewich J A, Heinz T F. Measurement of the optical conductivity of graphene. Physical Review Letters, 2008, 101(19): 196405

79. Novoselov K S, Fal'ko V I, Colombo L, Gellert P R, Schwab M G, Kim K. A roadmap for graphene. Nature, 2012, 490(7419): 192–200

80. Xing G, Guo H, Zhang X, Sum T C, Huan C H. The physics of ultrafast saturable absorption in graphene. Optics Express, 2010, 18(5): 4564–4573

81. Sun D, Wu Z K, Divin C, Li X, Berger C, de Heer W A, First P N, Norris T B. Ultrafast relaxation of excited Dirac fermions in epitaxial graphene using optical differential transmission spectroscopy. Physical Review Letters, 2008, 101(15): 157402

82. Dong P, Qian W, Liang H, Shafiiha R, Feng N N, Feng D, Zheng X, Krishnamoorthy A V, Asghari M. Low power and compact reconfigurable multiplexing devices based on silicon microring resonators. Optics Express, 2010, 18(10): 9852–9858

83. Balandin A A, Ghosh S, Bao W, Calizo I, Teweldebrhan D, Miao F, Lau C N. Superior thermal conductivity of single-layer graphene. Nano Letters, 2008, 8(3): 902–907

84. Gan X, Zhao C, Wang Y, Mao D, Fang L, Han L, Zhao J. Graphene-assisted all-fiber phase shifter and switching. Optica, 2015, 2(5): 468–471

85. Wang Y, Gan X, Zhao C, Fang L, Mao D, Xu Y, Zhang F, Xi T, Ren L, Zhao J. All-optical control of microfiber resonator by graphene's photothermal effect. Applied Physics Letters, 2016, 108(17): 171905

86. Qiu C, Yang Y, Li C, Wang Y, Wu K, Chen J. All-optical control of light on a graphene-on-silicon nitride chip using thermo-optic effect. Scientific Reports, 2017, 7(1): 17046

87. Tielrooij K J, Hesp N C H, Principi A, Lundeberg M B, Pogna E A A, Banszerus L, Mics Z, Massicotte M, Schmidt P, Davydovskaya D, Purdie D G, Goykhman I, Soavi G, Lombardo A, Watanabe K, Taniguchi T, Bonn M, Turchinovich D, Stampfer C, Ferrari A C, Cerullo G, Polini M, Koppens F H L. Out-of-plane heat transfer in van der Waals stacks through electron-hyperbolic phonon coupling. Nature Nanotechnology, 2018, 13(1): 41–46

88. Soref R, Bennett B. Electrooptical effects in silicon. IEEE Journal of Quantum Electronics, 1987, 23(1): 123–129

89. Weis P, Garcia-Pomar J L, Höh M, Reinhard B, Brodyanski A, Rahm M. Spectrally wide-band terahertz wave modulator based on optically tuned graphene. ACS Nano, 2012, 6(10): 9118–9124

90. Wen Q Y, Tian W, Mao Q, Chen Z, Liu W W, Yang Q H, Sanderson M, Zhang H W. Graphene based all-optical spatial terahertz modulator. Scientific Reports, 2014, 4(1): 7409

91. Zhang H, Virally S, Bao Q, Ping L K, Massar S, Godbout N, Kockaert P. Z-scan measurement of the nonlinear refractive index of graphene. Optics Letters, 2012, 37(11): 1856–1858

92. Yu S, Wu X, Chen K, Chen B, Guo X, Dai D, Tong L, Liu W, Ron Shen Y. All-optical graphene modulator based on optical Kerr phase shift. Optica, 2016, 3(5): 541–544

93. Sun Z, Hasan T, Torrisi F, Popa D, Privitera G, Wang F, Bonaccorso F, Basko D M, Ferrari A C. Graphene mode-locked ultrafast laser. ACS Nano, 2010, 4(2): 803–810

94. Bao Q, Loh K P. Graphene photonics, plasmonics, and broadband optoelectronic devices. ACS Nano, 2012, 6(5): 3677–3694

95. Marini A, Cox J D, García De Abajo F J. Theory of graphene saturable absorption. Physical Review B, 2017, 95(12): 125408

96. Brida D, Tomadin A, Manzoni C, Kim Y J, Lombardo A, Milana S, Nair R R, Novoselov K S, Ferrari A C, Cerullo G, Polini M. Ultrafast collinear scattering and carrier multiplication in graphene. Nature Communications, 2013, 4: 1987

97. Hanson G W. Dyadic Green's functions and guided surface waves for a surface conductivity model of graphene. Journal of Applied Physics, 2008, 103(6): 064302

98. Tielrooij K J, Piatkowski L, Massicotte M, Woessner A, Ma Q, Lee Y, Myhro K S, Lau C N, Jarillo-Herrero P, van Hulst N F, Koppens F H L. Generation of photovoltage in graphene on a femtosecond timescale through efficient carrier heating. Nature Nanotechnology, 2015, 10(5): 437–443

99. Soavi G, Wang G, Rostami H, Tomadin A, Balci O, Paradisanos I, Pogna E A A, Cerullo G, Lidorikis E, Polini M, Ferrari A C. Hot electrons modulation of third-harmonic generation in graphene. ACS Photonics, 2019, 6(11): 2841–2849

100. Song J C W, Tielrooij K J, Koppens F H L, Levitov L S. Photoexcited carrier dynamics and impact-excitation cascade in graphene. Physical Review B, 2013, 87(15): 155429

101. Dawlaty J M, Shivaraman S, Chandrashekhar M, Rana F, Spencer M G. Measurement of ultrafast carrier dynamics in epitaxial graphene. Applied Physics Letters, 2008, 92(4): 042116

102. Trushin M, Grupp A, Soavi G, Budweg A, De Fazio D, Sassi U, Lombardo A, Ferrari A C, Belzig W, Leitenstorfer A, Brida D. Ultrafast pseudospin dynamics in graphene. Physical Review B, 2015, 92(16): 165429

103. Song J C, Reizer M Y, Levitov L S. Disorder-assisted electron-phonon scattering and cooling pathways in graphene. Physical Review Letters, 2012, 109(10): 106602

104. Li W, Chen B, Meng C, Fang W, Xiao Y, Li X, Hu Z, Xu Y, Tong L, Wang H, Liu W, Bao J, Shen Y R. Ultrafast all-optical graphene modulator. Nano Letters, 2014, 14(2): 955–959

105. Tomadin A, Hornett S M, Wang H I, Alexeev E M, Candini A, Coletti C, Turchinovich D, Kläui M, Bonn M, Koppens F H L, Hendry E, Polini M, Tielrooij K J. The ultrafast dynamics and conductivity of photoexcited graphene at different Fermi energies. Science Advances, 2018, 4(5): eaar5313

106. Mikhailov S A. Theory of the strongly nonlinear electrodynamic response of graphene: a hot electron model. Physical Review B, 2019, 100(11): 115416

107. Tian W C, Li W H, Yu W B, Liu X H. A review on lattice defects in graphene: types, generation, effects and regulation. Micromachines, 2017, 8(5): 163

108. George P A, Strait J, Dawlaty J, Shivaraman S, Chandrashekhar M, Rana F, Spencer M G. Ultrafast optical-pump terahertz-probe spectroscopy of the carrier relaxation and recombination dynamics in epitaxial graphene. Nano Letters, 2008, 8(12): 4248–4251

109. Majumdar A, Kim J, Vuckovic J, Wang F. Electrical control of silicon photonic crystal cavity by graphene. Nano Letters, 2013, 13(2): 515–518

110. Fan K, Suen J, Wu X, Padilla W J. Graphene metamaterial modulator for free-space thermal radiation. Optics Express, 2016, 24(22): 25189–25201

111. Zeng B, Huang Z, Singh A, Yao Y, Azad A K, Mohite A D, Taylor A J, Smith D R, Chen H T. Hybrid graphene metasurfaces for high-speed mid-infrared light modulation and single-pixel imaging. Light, Science & Applications, 2018, 7(1): 51

112. Gan X, Mak K F, Gao Y, You Y, Hatami F, Hone J, Heinz T F, Englund D. Strong enhancement of light-matter interaction in graphene coupled to a photonic crystal nanocavity. Nano Letters, 2012, 12(11): 5626–5631

113. Shi Z, Gan L, Xiao T, Guo H, Li Z. All-optical modulation of a graphene-cladded silicon photonic crystal cavity. ACS Photonics, 2015, 2(11): 1513–1518

114. Liu Z B, Feng M, Jiang W S, Xin W, Wang P, Sheng Q W, Liu Y G, Wang D N, Zhou W Y, Tian J G. Broadband all-optical modulation using a graphene-covered-microfiber. Laser Physics Letters, 2013, 10(6): 065901

115. Chen J H, Zheng B C, Shao G H, Ge S J, Xu F, Lu Y Q. An all-optical modulator based on a stereo graphene–microfiber structure. Light, Science & Applications, 2015, 4(12): e360

116. Yu S L, Meng C, Chen B, Wang H, Wu X, Liu W, Zhang S, Liu Y, Su Y, Tong L. Graphene decorated microfiber for ultrafast optical modulation. Optics Express, 2015, 23(8): 10764–10770

117. Meng C, Yu S L, Wang H Q, Cao Y, Tong L M, Liu W T, Shen Y R. Graphene-doped polymer nanofibers for low-threshold nonlinear optical waveguiding. Light, Science & Applications, 2015, 4(11): e348

118. Zhang H, Healy N, Shen L, Huang C C, Hewak D W, Peacock A C. Enhanced all-optical modulation in a graphene-coated fibre with low insertion loss. Scientific Reports, 2016, 6(1): 23512

119. Debnath P C, Uddin S, Song Y W. Ultrafast all-optical switching incorporating in situ graphene grown along an optical fiber by the evanescent field of a laser. ACS Photonics, 2018, 5(2): 445–455

120. Romagnoli M, Sorianello V, Midrio M, Koppens F H L, Huyghebaert C, Neumaier D, Galli P, Templ W, D'errico A, Ferrari A C. Graphene-based integrated photonics for next-generation datacom and telecom. Nature Reviews Materials, 2018, 3(10): 392–414

121. Yu L, Zheng J, Xu Y, Dai D, He S. Local and nonlocal optically induced transparency effects in graphene-silicon hybrid nanophotonic integrated circuits. ACS Nano, 2014, 8(11): 11386–11393

122. Sun F, Xia L, Nie C, Shen J, Zou Y, Cheng G, Wu H, Zhang Y, Wei D, Yin S, Du C. The all-optical modulator in dielectric-loaded waveguide with graphene-silicon heterojunction structure. Nanotechnology, 2018, 29(13): 135201

123. Sun F, Xia L, Nie C, Qiu C, Tang L, Shen J, Sun T, Yu L, Wu P, Yin S, Yan S, Du C. An all-optical modulator based on a graphene–plasmonic slot waveguide at 1550 nm. Applied Physics Express, 2019, 12(4): 042009

124. Wang H, Yang N, Chang L, Zhou C, Li S, Deng M, Li Z, Liu Q, Zhang C, Li Z, Wang Y. CMOS-compatible all-optical modulator based on the saturable absorption of graphene. Photonics Research, 2020, 8(4): 468

125. Ono M, Taniyama H, Xu H, Tsunekawa M, Kuramochi E, Nozaki K, Notomi M. Deep-subwavelength plasmonic mode converter with large size reduction for Si-wire waveguide. Optica, 2016, 3(9): 999–1005

126. Ruzicka B A, Wang S, Werake L K, Weintrub B, Loh K P, Zhao H. Hot carrier diffusion in graphene. Physical Review B, 2010, 82 (19): 195414

127. Zhu J, Cheng X, Liu Y, Wang R, Jiang M, Li D, Lu B, Ren Z. Stimulated Brillouin scattering induced all-optical modulation in graphene microfiber. Photonics Research, 2019, 7(1): 8–13

128. Wang Y, Zhang F, Tang X, Chen X, Chen Y, Huang W, Liang Z, Wu L, Ge Y, Song Y, Liu J, Zhang D, Li J, Zhang H. All-optical phosphorene phase modulator with enhanced stability under ambient conditions. Laser & Photonics Reviews, 2018, 12(6): 1800016

129. Koppens F H, Chang D E, García de Abajo F J. Graphene plasmonics: a platform for strong light-matter interactions. Nano Letters, 2011, 11(8): 3370–3377

130. Ooi K J A, Tan D T H. Nonlinear graphene plasmonics. Proceedings of the Royal Society of London, Series A, 2017, 473(2206): 20170433

Junying Li is a postdoctoral fellow at College of Optical-electrical and Computer Engineering, University of Shanghai for Science and Technology, Shanghai, China. She received her B.S. degree in Optoelectronic Engineering in 2013, and Ph.D. degree in Optical Engineering in 2018, both from Chongqing University, Chongqing, China. Dr. Li's research focuses on chalcogenide phase change materials, chalcogenide integrated photonics, and surface-enhanced Raman scattering. She has authored and co-authored more than 20 journal publications, including publications in *Nature Communication*, *Carbon*, etc.

Hongtao Lin is an Assistant Professor at College of Information Science and Electronic Engineering, Zhejiang University, Hangzhou, China. He received his B.S. degree in Materials Physics from University of Science and Technology of China, Hefei, China, in 2010, and Ph.D. degree in Materials Science from University of Delaware, Newark, DE, USA, in 2015. His research interests are focused on chalcogenide integrated nanophotonics and their applications for mid-infrared sensing/communication, flexible and wearable photonics, two-dimensional materials optoelectronics.

Dr. Lin has authored and co-authored more than 40 referred journal publications and more than 30 conference proceedings, including publications in *Nature Photonics*, *Nature Communication*, *Optica*, etc. His works had been selected to be included in "Optics in 2014" and "Optics in 2018" by OSA's Optic & Photonics News.

Chuyu Zhong is a post-doctor at College of Information Science and Electronic Engineering, Zhejiang University, Hangzhou, China. He received his B.S. degree in Theoretical Physics from Wuhan University, Wuhan, China, in 2013, and Ph.D. degree from Changchun Institute of Optics, Fine Mechanics and Physics, Changchun, China, in 2018. Dr. Zhong had made his contribution to the research of vertical-cavity surface-emitting laser (VCSEL). His current research interests are focused on silicon photonics and chalcogenide integrated nanophotonics, and their applications include mid-infrared modulation and graphene-based optoelectronics.